International Journal of Heat and Mass Transfer 70 (2014) 330–339

Contents lists available at ScienceDirect

International Journal of Heat and Mass Transfer

journal homepage: www.elsevier.com/locate/ijhmt

Genetic optimization of heat transfer correlations for evaporator tube flows

Matheus P. Porto [a,b], Hugo T.C. Pedro [b], Luiz Machado [a], Ricardo N.N. Koury [a], Carlos U.S. Lima [c], Carlos F.M. Coimbra [b,*]

[a] Programa de Pós Graduação em Engenharia Mecânica, Universidade Federal de Minas Gerais, Belo Horizonte, MG, Brazil
[b] Department of Mechanical and Aerospace Engineering, Jacobs School of Engineering, Center of Excellence in Renewable Energy Integration, Center for Energy Research University of California San Diego, La Jolla, CA, USA
[c] Departamento de Engenharia Mecânica, Universidade Federal do Pará, Belém, PA, Brazil

ARTICLE INFO

Article history:
Received 6 June 2013
Received in revised form 4 November 2013
Accepted 5 November 2013
Available online 30 November 2013

Keywords:
Heat transfer coefficient
Internal flows
Genetic algorithms
Artificial neural networks

ABSTRACT

Two-phase heat transfer coefficients for internal flows play a critical role in the design and analysis of evaporators and condensers. Previous studies propose empirical relations that combine the effects of nucleate and convective boiling onto the overall heat transfer coefficient. Although these relatively simple empirical relations offer physical insight on the nucleation, boiling and flow processes, they come at the expense of some computational accuracy. In this work, we explored new techniques to determine two-phase heat transfer coefficients for refrigerants R-22, R-134a and R-404a. We used multiple functional forms for the heat transfer coefficients and considered multiple dimensionless parameters as inputs to the algebraic relations. We used genetic algorithms to search the solution space that consists of the input parameters plus the different functional forms, and obtained optimal empirical correlations that cover a wide range of heat transfer regimes. Then, we combined genetic algorithm and artificial neural networks to obtain a more universal correlation. Two versions were developed for each correlation: one that assumes a priori knowledge of the local heat flux and another that does not. Several error metrics were computed for all the correlations developed and compared against correlations from the literature. We conclude that substantial improvements can be achieved in both accuracy and robustness of the correlations by using advanced optimization techniques.

1. Introduction

The determination of the heat transfer coefficients (HTC) in phase-changing conditions is critical to the optimal design of refrigeration systems. The current level of computational technology allows for the use of computationally intensive tools to solve heat transfer problems that were beyond reach just a few decades ago. Two optimization tools that are particularly relevant to the optimal determination of two-phase flow coefficients are genetic algorithms (GAs) and artificial neural networks (ANNs). Recent works employing GAs for the solution of heat transfer problems are reviewed by Gosselin et al. [1]. Mojaraj et al.[2] reviewed the application of ANNs for refrigeration, air conditioning and heat pump systems (RACHP), highlighting the ANN ability to model and solve multivariable nonlinear problems. Considering the determination of HTC in particular, both ANNs and GAs have proven to offer substantial advantages over conventional methods for correlating experimental data [3–7]. Mohanraj et al. [2] conclude that there are substantial gains to be explored in the following areas:

- development of simplified correlations for predicting the performance of RACHP systems;
- hybridization of ANN with other expert systems;
- phase change behavior of newly developed refrigerant mixtures.

The present work introduces four different methodologies for obtaining two-phase flow HTC correlations, and these methodologies combine all three areas mentioned above. The first two are based on the optimization of strictly empirical algebraic expressions, the third results from the optimization of an HTC functional form currently in use (based on the asymptotic behavior of nonlinear superposition effects), and the last one is based on the ability of ANNs to function as a universal nonlinear approximator. With the exception of the third methodology, the other methodologies are applied to two distinct cases: (1) assuming that the heat flux is known, and (2) assuming that the heat flux is unknown. The second scenario has especial relevance in design applications for which both the heat fluxes and the wall temperatures are

* Corresponding author. Tel.: +1 (858) 534 4285; fax: +1 (858) 534 7599.
E-mail address: ccoimbra@ucsd.edu (C.F.M. Coimbra).

0017-9310/$ - see front matter © 2013 Elsevier Ltd. All rights reserved.
http://dx.doi.org/10.1016/j.ijheatmasstransfer.2013.11.011

Nomenclature

d	diameter, m
g	gravitational acceleration, m s^{-2}
G	mass flux, kg m^{-2} s^{-1}
h	heat transfer coefficient (HTC), W m^{-2} K^{-1}
i	enthalpy, kJ kg^{-1}
k	thermal conductivity, W m^{-1} K^{-1}
Q	heat flow, W
Q''	heat flux, W m^{-2}
U	mass flow or bulk velocity, m s^{-1}
RMSE	root mean square error, W m^{-2} K^{-1}
MAE	mean square error, W m^{-2} K^{-1}
MBE	mean bias error, W m^{-2} K^{-1}
R^2	coefficient of determination

Greek

χ	Martinelli parameter
μ	viscosity, Pa s
ρ	specific mass, kg m^{-3}
σ	surface tension, N m^{-1}

Dimensionless numbers

Fr	Froude number, $G^2\rho^{-2}g^{-1}d^{-1}$
Pr	Prandtl number, $\mu c_p K^{-1}$
Re	Reynolds number, $\rho U d/\mu$
We	Weber number, $G^2 d\rho^{-1}\sigma^{-1}$

Subscripts

cb	convective boiling
$crit$	critical properties
eq	equivalent property – linear proportion between saturation properties and quality
l	saturated liquid, $x = 0$
lv	difference between vapor from liquid saturated properties
nb	nucleate boiling
tp	two-phase flow
tt	liquid/vapor interface
s	saturated
v	saturated vapor, $x = 1$
w	tube wall

unknown. The selection of inputs to be considered for all the correlations was optimized via GA.

To develop the optimized HTCs, we used data from different refrigerants (R404a, R134a and R22), and different flow pattern conditions, that were obtained experimentally by varying the evaporation temperature, vapor quality, mass flow and heat flux.

2. Two-phase flow HTC correlations

The HTC in a horizontal tube can be determined experimentally through the convective heat transfer definition:

$$h = Q''/(T_w - T_s) \tag{1}$$

and

$$Q'' = Q/S, \tag{2}$$

where h is the HTC (W m^{-2} K^{-1}), Q'' is the heat flux (W m^{-2}), T_w is the tube internal surface temperature (°C), T_s is the bulk temperature of the fluid (°C), and S is the tube surface area (m^2).

Understanding the different phase change flow regimes is critical to the development of optimal HTC correlations. Phase changing has multiple roles in RACHP, and what is particularly relevant in our study is the enhancing mechanism for heat transfer capacity. In general, heat transfer rates during phase change can be 4 to 25 times higher than for equivalent single-phase forced convection [8]. Fig. 1 describes the most relevant flow patterns and HTC levels during the phase change process along an evaporator tube. The flow pattern presented in this figure is only illustrative and it will vary depending on the fluid characteristics and flow regimes (evaporation temperature, vapor pressure, heat flux, mass flow velocity, diameter and vapor quality, etc.). Observing the evolution of HTC regimes along the evaporator it is possible to recognize:

- a gradual increase in HTC due to the phase change phenomena, related to nucleate and convection boiling;
- a rapid decrease for high values of quality, more precisely in the region identified as dryout/mist flow.

The phase change mechanism can be further divided into two different processes: convection boiling, which is the phase change regime that occurs in the liquid/vapor interface; and nucleate boiling, which is the phase change regime related to bubble formation on a heated surface (liquid/solid interface). There is a group of correlations, called Strictly Convective, that considers only the convection term for the calculation of a two-phase flow HTC [9–14]. In general, Strictly Convective correlations use the well-known Dittus–Boelter heat transfer relation applied to saturated liquid flow and the Martinelli parameter [15], as expressed by

$$h_{tp} = h_l(1 + C_l\chi_{tt})^{-C_2}, \tag{3}$$

where C_1 and C_2 are constants obtained empirically, as proposed by Bandarra [14]. Another group of correlations, called Superposition Rule correlations, considers both processes: convection boiling (h_{cb}) and nucleation boiling (h_{nb}) [16–22]. These correlations determine the functional form of the HTC by weighing the contribution of each mechanism of heat transfer (h_{nb} and h_{cb}) as

$$h_{tp} = \left[(Fh_{cb})^n + (Sh_{nb})^n\right]^{1/n}. \tag{4}$$

where S and F are weighing factors for the two components. At high values of mass flow the temperature gradient near the wall

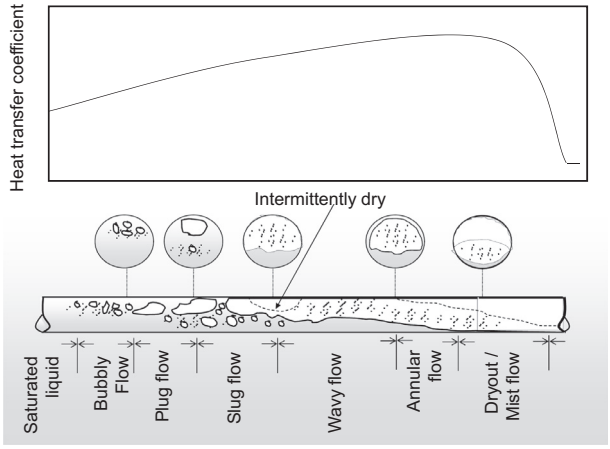

Fig. 1. Example of phase change HTC and flow patterns for a fluid passing through a tube evaporator.

increases as consequence of a thinner boundary layer. The effective temperature around bubbles also decreases reducing the chances of bubble formation. In this situation the suppression factor S becomes smaller. Likewise at high vapor quality flow regimes there is a smaller chance of bubble formation, and the suppression factor S should again decrease. Otherwise, the convective heat transfer should increase for high values of quality and mass flow, and the factor F, composed by the Martinelli parameter χ should express it. When the parameter n is not one, the weighing is biased, and the result tends to become closer to the largest value among the two terms. Generally speaking, Superposition Rule correlations produce more robust and useful approximations than Strictly Convective correlations.

A third group of two-phase flow approximations for HTCs is the so-called strictly empirical [23–25]. For these approximations dimensionless numbers are correlated to experimental data using numerical methods for optimizing the coefficients in the expressions. This technique has gained popularity [1,2] with the increase of computational power in recent years that enables testing large quantities of dimensionless numbers and increasingly larger data sets.

The fourth group of HTCs is closely related to the flow pattern map. As shown in Fig. 1 there are substantial differences between the different flow regimes along the tube. For this reason several authors have investigated flow pattern maps and proposed HTC correlations for each flow pattern [26–32], instead of a single global correlation. Fig. 2 shows an example of flow pattern map implemented using the methodology presented by Wojtan et al. [31]. The subjective aspect of pattern determination [16] has been greatly mitigated by new methodologies, as presented by Ursenbacher et al. [33]. The main drawback of using Wojtan et al. [31,32] methodology is the assumption of a priori knowledge of the heat flux, which is typically what the designer is trying to determine in the first place.

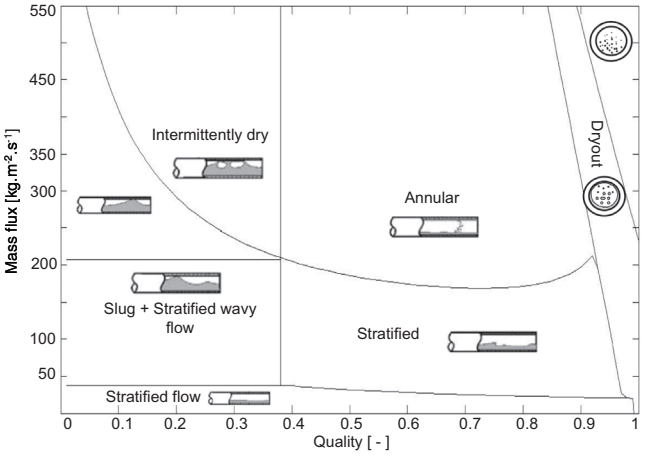

Fig. 2. Flow pattern map for refrigerant R-22 for saturation temperature of 8 °C, an internal diameter of 12.97 mm, and heat flux of 5 kW m^{-2}.

3. Experimental setup

Fig. 3 shows the schematic diagram of the experimental setup used in this work. To avoid contamination the refrigerant circuit was equipped with a gear micro-pump, which also allows for precise mass flow rate control. The flow patterns were observed through a window glass tube in the inlet and outlet of the test section. The ethylene glycol water and liquid cooler circuits were used to change the evaporation temperature in the refrigerant circuit. Heat flux was generated through electrical resistances (recently, counter current flow setups have gained some popularity because they achieve a more homogeneous boundary condition on the dry-out region). The temperature uncertainty is equal to 0.2 °C, pressure transmitter uncertainty is 0.3% of measured values, mass flow meter uncertainty is equal to 0.15% of the measurement, tube diameter is equal to 12.97 ± 0.05 mm and the length of the test section is 2001.2 ± 7.65 mm. Detailed information on this experimental test bench can be found in Lima [6]. This apparatus was used to measure 690 experimental data points for three different refrigerants: R22, R134a and R404a.

4. Methodology

This section describes the methodology used to generate the new correlations. The first step in this process was to create a set of inputs that may be included in the correlations. Table A.1 lists all the dimensionless numbers used in this work. The first group of inputs takes the form of dimensionless numbers based on several properties d, U, k, μ and i_{lv}, that were determined through the Buckinham Π theorem [7]. Other inputs consist of the enhancing factor S presented in Lima [6] (see correlation number 4, Table A.1), and the dimensionless numbers given by Wojtan et al. [31,32]. The parameters C_1, C_2 to C_5 were also used here in order to consider the influence of the critical thermophysical properties of the fluids in the HTC correlation.

The second step was to determine the functional form for the correlation. Given that it is impossible to know a priori what type of correlation performs best we explored four functional forms for

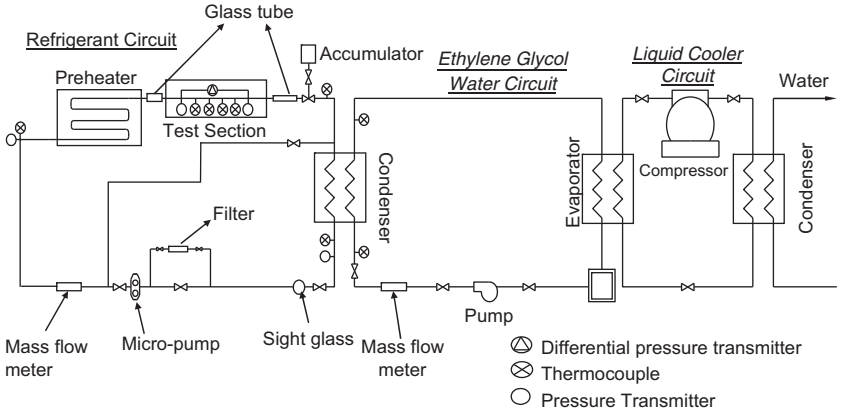

Fig. 3. Schematic diagram of the experimental setup.

the HTC correlations: two strictly empirical algebraic equations, an algebraic equation based on the Superposition Rule and a correlation based on ANNs. The two empirical algebraic correlations are given by:

$$h_{tp} = \left(\sum_{i=1}^{n_1} a_i X_i^{b_i}\right)\prod_{j=1}^{n_2} X_j^{c_j}, \tag{5}$$

$$h_{tp} = a_0\sum_{i=1}^{n_1} a_i X_i^{b_i} + c_0\prod_{j=1}^{n_2} X_j^{c_j}, \tag{6}$$

where the X's are a subset of the dimensionless parameters in Table A.1). The coefficients $a_i,\ b_i$ and c_j can be negative which means that these expressions can also include subtractions and divisions.

The third functional form is based on the Superposition Rule:

$$h_{tp} = \left[\left(a_0\sum_{i=1}^{n_1} a_i X_i^{b_i} + c_0\prod_{j=1}^{n_2} X_j^{c_j}\right)h_l^n + \left(d_0\sum_{i=1}^{n_3} d_i X_i^{e_i} + f_0\prod_{j=1}^{n_4} X_j^{f_j}\right)h_{nb}^n\right]^{1/n}, \tag{7}$$

where h_l is the correlation of Dittus–Boelter applied for saturated liquid flow and h_{nb} is the nucleate boiling HTC correlation presented by Cooper [34].

4.1. Artificial neural networks

The fourth type of correlation considered in this study is obtained through ANNs. ANNs are useful tools for approximating complicated mapping functions for problems in classification and regression [36] and have been used extensively in many areas. The advantage of ANNs is that no assumptions are required about the underlying process relating input and output variables. However, because ANNs are universal approximating functions, their mapping capabilities can potentially lead to problems such as over-fitting the training data [36] leading to poor results on new data sets. In this study the ANN is a representation of HTC in terms of a subset of the dimensionless parameters X. The ANN representation is based on signals being sent through elements called neurons in such a way that the processing of the inputs signals produces an output HTC or target value which in this case, are the experimental values for HTC. Neurons are arranged in layers, where the first layer contains the set of inputs, the last layer contains the output, and the layers in between (referred to as hidden layers) contain hidden neurons. The feedforward neural network that used here, with N_i inputs and N_h neurons in a single hidden layer and linear output activation function, can be expressed as

$$h_{tp} = a_0\left[\sum_{i=1}^{N_h} w_i f^h\left(\sum_{j=1}^{N_i} w_{ij}\widetilde{X}_j + w_{i0}\right) + w_0\right] + b_0, \tag{8}$$

where f_i^h is a transfer function and $\widetilde{X}_j$ is the jth dimensionless parameter normalized in the range $[-1, 1]$ using the range limits listed in Table A.1. Numerical optimization algorithms such as back-propagation, conjugate gradients, quasi-Newton, and Levenberg–Marquardt have been developed to efficiently adjust the weights, w_i and w_{ij}, and bias w_{i0} and w_0 in the feedforward neural network seeking to minimize a performance function like the mean squared error.

4.2. Model optimization

All the correlations presented are uniquely determined by the inputs X used and the several free coefficients ($a_i,\ b_i,\ c_i,\ w_{ij}$, etc). The best correlation for each one of the four types explored is the one that minimizes the root mean square error:

$$\underset{\vec{x},\vec{y}}{\operatorname{argmin}}\sqrt{\frac{1}{N}\sum_{i=1}^{N}\left(h_{tp,exp,i} - h_{tp,i}(\vec{x},\vec{y})\right)^2}, \tag{9}$$

where $h_{tp,exp}$ is the experimental HTC, and h_{tp} is the HTC computed by the new correlations defined by the vectors $\vec{x}$ and $\vec{y}$.

The vector $\vec{y}$ contains the coefficients $a_i, b_i, \ldots$ in the case of the algebraic correlations or the weights and bias $w_{ij},\ w_{i0}$ in the case of the ANN-based correlation. For the algebraic correlations the coefficients $a_i, b_i, \ldots$ were determined using an unconstrained line-search method [35] implemented in Matlab R2012b (accessible through the Optimization toolbox via the function *fminunc*). For the ANN-based correlations w_{ij} and w_{i0} are determined using the Levenberg–Marquardt algorithm implemented by the Neural Network Toolbox in Matlab R2012b.

The vector $\vec{x}$ is a binary vector whose elements determine the inclusion ($x_i = 1$) or exclusion ($x_i = 0$) of the dimensionless parameters X_i. In the case of Eqs. (5)–(7) each input can appear multiple times, once for each term. For the ANN-based correlation the final correlation also depends on the number of neurons and the type of transfer function used. These two parameters are defined by two integers appended to $\vec{x}$. The first, in the range $[5, 20]$, determines the number of neurons N_h in the hidden layer. The second, in the range $[1, 4]$, is used to select the transfer function f^h out of 4 possibilities: hyperbolic tangent sigmoid transfer function, log-sigmoid transfer function, radial basis transfer function and the linear transfer function.

Unlike for $\vec{y}$, gradient-based optimization methods are not suited for determining the optimal $\vec{x}$ because it is not possible to compute the gradient of Eq. (9) with respect to $\vec{x}$. For this reason, we employed GA to determine the best input selection and ANN architecture, i.e, the best $\vec{x}$.

Table 1
Description of GA settings and search space $\vec{x}$.

GA settings		
Selection	Stochastic uniform	
Cross-over	Scatter	Randomly selects entries from the parents
Mutation	Uniform	5% mutation probability
Elitism	Yes	2 Individuals
Population size	100	
Max. generations	100	
Initial population	Random	
GA search space (*description of* $\vec{x}$)		
Eqs.	No. elements	Description
(5) and (6)	50 (52)[a]	Binary values for input selection
(7)	−(104)	Binary values for input selection
(8)	25 (26) + 2 (2)	Binary values for input selection + two integer values for number of neurons and transfer function selection

[a] Values in parentheses refer to the correlation that include the *Bo* number, otherwise they refer to the correlations with no *Bo* number.

4.3. Genetic algorithms

The GA is a space search technique based on the mechanism of natural selection and survival of the fittest [37]. In this algorithm the evolution starts with a random population of individuals (determined by vectors $\vec{x}$). Each individual in the population is ranked according to the RMSE, between the experimental and the calculated HTC values. The initial population is evolved based on the selection, crossover and mutation operators with the objective to minimize RMSE. Crossover operates on individuals (parents) determined by the selection operator that selects individuals for crossover based on fitness. Here we used the stochastic uniform methods to select individuals for crossover, in this method the probability of selection is proportional to the individuals fitness. Crossover recombines the genetic material of the selected parents. We used the scattered method in which a random binary vector with the same length as $\vec{x}$ is used to select the elements coming from each parent. The crossover operator selects elements from the first parent where the vector has 0 entries and selects genes from the second parent when it has 1 entry. The mutation operator modifies individuals that have not been selected for reproduction by randomly changing $\vec{x}$. In this work we used the uniform mutation algorithm that selects a fraction of the vector $\vec{x}$ for mutation. Each one of the selected entries has a 5% probability of being mutated. Mutated entries are replaced by a uniformly random value. Once the population for a new generation is determined this process continues until some criterion is met. Given that it is difficult to formally specify a convergence criterion for GA due to its stochastic nature, in this work the algorithm stopped after 100 generations or if no improvement was observed over a pre-specified number of generations, in this case 50.

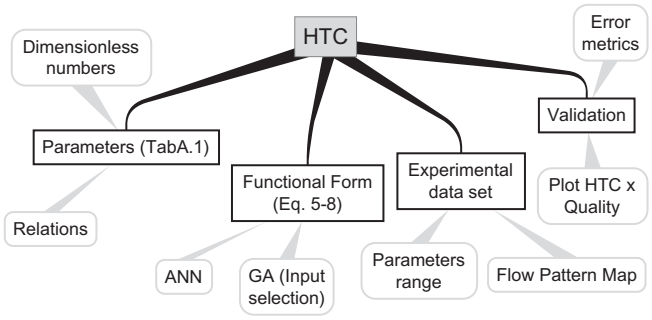

Fig. 4. Methodology for obtaining optimal HTC correlations.

Table 1 lists the GA settings used in this work and describes the GA search space, i.e., the components of vector $\vec{x}$, for the 4 types of correlations and 2 types of inputs (with *Bo* and without *Bo*). The GA tools used in this work are the ones implemented in the Global

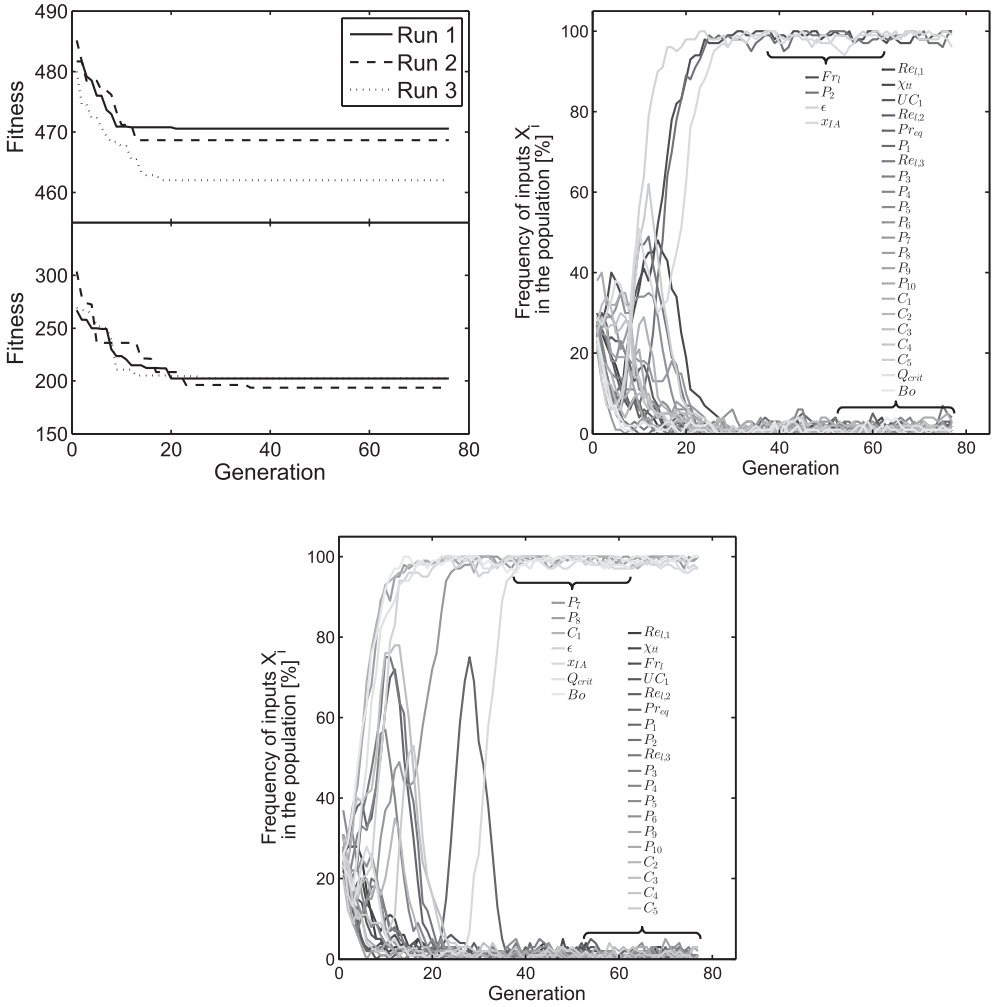

Fig. 5. Left: fitness value of the best individual versus the generation number for three runs for the correlations HTC2$_a$ (top) and HTC2$_b$ (bottom). Middle: evolution of the frequency of inputs X_i in the summation term of HTC2$_b$ (Eq. (6)) versus the GA generations for the third run. Right: same as (b) but for the multiplication term.

Table 2
Optimized algebraic correlations.

Correlation	Equation	Coefficients
$HTC1_a$	$\left(a_1 UC_1^{b_1} + a_2 P_7^{b_2} + a_3 P_8^{b_3} + a_4 C_1^{b_4} + a_5 x_{lA}^{b_5}\right) \times Fr_l^{c_1} UC_1^{c_2} P_2^{c_3} Re_{l,3}^{c_4} P_7^{c_5} C_2^{c_6} C_3^{c_7} C_5^{c_8} \varepsilon^{c_9}$	$a = \{1.908, -2.102, 1.105, 2.303, -0.642\}$, $b = \{1.666, 2.857, 0.251, 1.246, 0.507\}$, $c = \{0.789, 0.207, 1.569, -2.431, -1.240, -2.539, 1.643, -0.148, 2.478\}$
$HTC1_b$	$\left(a_1 P_8^{b_1} + a_2 P_9^{b_2} + a_3 C_2^{b_3} + a_4 Bo^{b_4}\right) \times Pr_{eq}^{c_1} P_1^{c_2} P_{10}^{c_3} C_1^{c_4} C_2^{c_5} C_4^{c_6} C_5^{c_7} \varepsilon^{c_8} x_{lA}^{c_9} Bo^{c_{10}}$	$a = \{-0.035, 1.235, -0.001, 1.411\}$, $b = \{2.219, -0.639, 1.707, 1.037\}$, $c = \{0.008, -0.359, -0.763, 0.851, -1.651, 5.312, 0.586, -0.666, -0.577, -0.402\}$
$HTC2_a$	$a_0\left(a_1 \chi_{tt}^{b_1} + a_2 Fr_l^{b_2} + a_3 \varepsilon^{b_3}\right) + c_0 Fr_l^{c_1} Pr_{eq}^{c_2} P_2^{c_3} Re_{l,3}^{c_4} P_8^{c_5} C_3^{c_6} C_5^{c_7}$	$a = \{-468.813, -456.456, 0.107, 3.671\}$, $b = \{-2123.082, 6.226, 5.344\}$, $c = \{0.023, 0.995, 0.007, -0.381, 1.955, -2.072, -0.044, -0.018\}$
$HTC2_b$	$a_0\left(a_1 Fr_l^{b_1} + a_2 P_2^{b_2} + a_3 \varepsilon^{b_3} + a_4 x_{lA}^{b_4}\right) + c_0 P_7^{c_1} P_8^{c_2} C_1^{c_3} \varepsilon^{c_4} x_{lA}^{c_5} Q_{crit}^{c_6} Bo^{c_7}$	$a = \{141.452, 220.465, 137.852, -184.078, -175.476\}$, $b = \{0.009, -0.262, -0.083, 1.005\}$, $c = \{16.488, 0.236, 0.007, 2.851, -0.296, -5.968, 0.553, 0.217\}$
HTC3	$\left[\left(a_0\left(a_1 \chi_{tt}^{b_1} + a_2 UC_1^{b_2} + a_3 Pr_{eq}^{b_3}\right) + c_0 Fr_l^{c_1} C_3^{c_2}\right) h_l^n + \left(d_0 (d_1 P_7^{e_1} + d_2 C_2^{e_2} + d_3 C_3^{e_3} + d_4 \varepsilon^{e_4}) + f_0 Fr_l^{f_1} Pr_{eq}^{f_2} \varepsilon^{f_3}\right) h_{nb}^n\right]^{1/n}$	$a = \{2.468, 0.156, 1.093, 0.756\}$, $b = \{1.967, 0.230, 1.410\}$, $c = \{-3.205, 0.887, 0.282\}$, $d = \{1.248, 0.200, 8.925, -0.504, 0.468\}$, $e = \{-0.485, 2.504, 0.484, -0.407\}$, $f = \{-0.440, 3.923, 0.473, 16.827\}$, $n = 1.713$

Optimization Toolbox (Version 3.2.2) in Matlab R2012b. Fig. 4 summarizes the different procedures used in this work to develop and validate the HTC correlations.

5. Results and discussion

The GA optimization was performed for 7 different cases: the 3 correlations defined by Eqs. (5), (6) and (8) with and without considering *Bo* as one of the possible inputs, and the correlation given by Eq. (7). These 7 correlations are identified as $HTC1_a$, $HTC1_b$ for the correlations in the form of Eq. (5), $HTC2_a$, $HTC2_b$ for the correlations in the form of Eq. (6), and HTC3 for the correlations in the form of Eq. (7), and $HTC4_a$, $HTC4_b$ for the correlation in the form of Eq. (7). The subscript *a* denotes that *Bo* was not used and the subscript *b* denotes otherwise.

In all 7 GA runs we started with a uniformly random population, which means that all the possible inputs are equally represented in the initial population. Given the random nature of the GA we ran each optimization three times. For the algebraic correlations the GA converges rapidly as illustrated by Fig. 5(a), corresponding to the optimization of correlations $HTC2_a$ and $HTC2_b$. In most cases all the runs converge to approximately the same value which assures us that the GA is returning a solution near the global optimum.

The Fig. 5(b) and (c) show the frequency of inputs X_i in the summation and multiplication terms of correlation $HTC2_b$ for a given generation. If the frequency of a given input is close to 100% that means that all correlations being tested use that input. These figures show that after 40 generations the input selection has converged to a small set of inputs (Fr_l, P_2, ε, x_{lA} for the summation term and P_7, P_8, C_1, ε, x_{lA}, Q_{crit}, Bo for the multiplication term). In the remaining generations the GA tries to find the best combination of inputs from these sets that returns the best correlations.

The best algebraic expressions are listed in Table 2. As explained before, the set of dimensionless numbers used as inputs was determined by the GA and the free coefficients were obtained with the minimization function *fminunc*. The best parameters for the ANN-based models are listed in Table 3. The values of weights and bias for the two ANN expressions that use the normalized inputs listed in Table 3 in Eq. (8) are listed in Tables A.2 and A.3 in Appendix.

Table 2 shows that the void fraction ε appears in all correlations. This is because the void fraction has direct influence on the dry angle and HTC [31]. The Martinelli parameter appears in equation HTC3 in the same way that it appears in most correlations based on the Superposition Effects rule, reinforcing the dependence between the Martinelli parameter and the convective boiling term. Likewise the Froude number that appears in several Superposition Effects rule correlations [16,18–22], also appears in most of the correlations in Table 2.

As explained above, the single objective of the optimization problem described by Eq. (9) was to minimize the RMSE between the experimental data and the new correlations. Given that a multi-objective optimization involving other error metrics was not performed in this study, it is possible that the optimized correlations have low RMSE but high bias or dispersion when compared to existent correlations. Thus, in order to fully assess the performance of the different correlations, we computed several error metrics (defined in Appendix A.1) for the difference between the experimental HTC and one computed with the new correlations. These values are summarized in Table 4. In this table we also show the error metrics for correlations by Kandlikar [24] and Wattelet [20]. Almost all the optimized correlations show smaller MBE, MAE and RMSE than these 2 correlations. However in terms of

Table 4
Error metrics for the different correlations. Values calculated with complete set of experimental data.

Correlation	MBE	MAE	RMSE	R^2
$HTC1_a$	−1.64	375.24	457.38	0.56
$HTC1_b$	−0.05	99.19	141.06	0.96
$HTC2_a$	−37.45	385.64	462.73	0.56
$HTC2_b$	−33.11	131.78	175.19	0.94
HTC3	−2.10	98.15	136.95	0.96
$HTC4_a$	−0.35	359.05	440.84	0.60
$HTC4_b$	3.45	57.62	94.41	0.98
Kandlikar	−509.69	621.3	820.23	0.71
Wattelet	−33.84	357.71	467.4	0.75

Table 3
Best parameters for the ANN correlations $HTC4_a$ and $HTC4_b$.

Correlation	Inputs	N_h	f^h	a_0	b_0
$HTC4_a$	χ_{tt}, Fr_l, P_1, $Re_{l,3}$, P_6, P_8, C_1, C_2, C_5, Q_{crit}	6	Tansig[a]	1985.64	1987.37
$HTC4_b$	$Re_{l,1}$, χ_{tt}, Fr_l, $Re_{l,2}$, Pr_{eq}, P_1, P_2, $Re_{l,3}$, P_3, P_4, P_6, P_8, C_1, C_2, C_3, x_{lA}, Bo	7	Tansig	1985.64	1987.37

[a] Hyperbolic tangent sigmoid: tansig $(x) = 2/[1 + \exp(-2 * x)] - 1$.

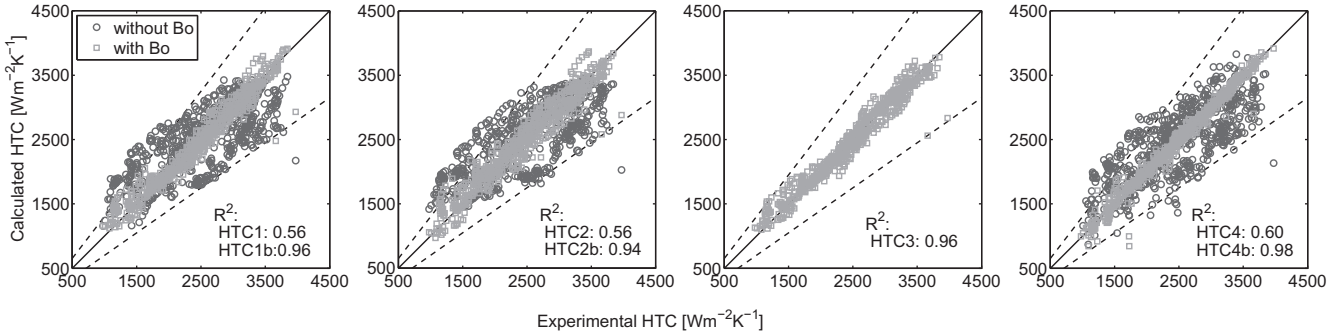

Fig. 6. Scatter plots of experimental HTC versus calculated HTC. The correlations used to calculate HTC were (from left to right): HTC1$_a$ and HTC1$_b$, HTC2$_a$) and HTC2$_b$, HTC3, and HTC4$_a$ and HTC4$_b$. The dashed lines identify a deviation of 30% between the experimental and the calculated HTC values.

dispersion (as measured by R^2) the proposed models that do not use *Bo* (the ones identified by the subscript *a*) are substantially worse than those by Kandlikar and Wattelet (which use *Bo* or the wall heat flux as one of the inputs). If the boiling number *Bo* is available the accuracy of the new correlations (the ones identified by the subscript *b* and the third correlation) improve greatly, reducing the MAE and RMSE by at least 60% and increasing the R^2 values to above 0.94. Fig. 6 shows the experimental HTC versus the calculated HTC for the 7 correlations developed here. These plots demonstrate clearly the improvement in the correlation accuracy when *Bo* is available.

Table 5
Experimental parameters used by different authors for measuring two-phase heat transfer coefficients.

Correlation	Kandlikar [24]	Wattelet [20]	Present work
Fluids in common	R22, R134a	R22, R134a	R22, R134a and R404a
Mass Flux (kg m^{-2} s^{-1})	[15,8180]	[25,500]	[50,500]
Temperature (°C)	[0.8,8]	[−15.3,20.3]	[8,15]
Quality (–)	[0.1,0.95]	[0.1,0.9]	[0.01,0.94]
Heat flux (kW m^{-2})	[1.2,2000]	[2,30]	[1.9,40]

In the previous error analysis we applied the new correlations to the entire data set of experimental values. These include data points from multiple fluids and flow patterns. To further assess the accuracy and the behavior of the correlations we studied how HTC varies against the two-phase flow quality for a single fluid, and compared them against the correlations by Kandlikar and Wattelet. To guarantee that all the correlations can be compared fairly Table 5 lists the experimental conditions under which they were obtained. The table shows that all the analyzed correlations have used R-22 as a common working fluid, thus in the following analysis only data points for R-22 were considered.

The relative low mass and heat flux ranges used in our experiments result from using the micro-pump in order to avoid contamination and improve the quality of the results. In terms of mass flow rate and the flow patterns our experiments can be grouped as:

- low mass flow rate (100 kg m^{-2} s^{-1}): predominantly slug and stratified wavy flow for lower quality ($x < 0.4$, approximately) and stratified wavy flow for higher quality – see Fig. 7(a)-top;
- medium mass flow rate (200 kg m^{-2} s^{-1}): transition between slug and slug plus stratified wavy flow for lower quality and annular for higher quality – see Fig. 7(b)-top;

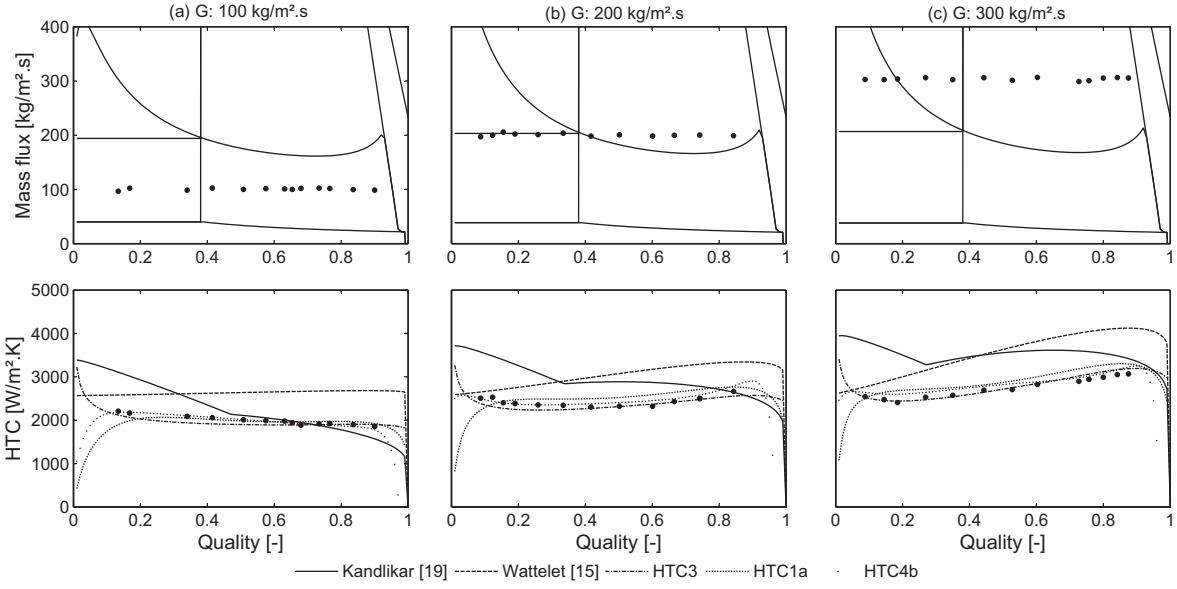

Fig. 7. Top: Flow pattern map and experimental points for the fluid R-22. Bottom: comparison between different methodologies for determining the HTC for R-22. The large black dots represent the experimental data.

- high mass flow (above 300 kg m^{-2} s^{-1}): slug and intermittently dry for lower quality and annular for higher quality – see Fig. 7(c)-top.

At the bottom row of Fig. 7 we plotted the HTC values versus the two-phase flow quality using the correlations HTC1$_a$, HTC3, and HTC4$_b$ listed above, and the correlations by Kandlikar and Wattelet. The Wattelet correlation shows a behavior that is very close to the one from our experimental data for the three cases shown here, although it also shows a large positive bias. Kandlikar correlation performs poorly for low vapor qualities but it matches the experimental better than Wattelet correlation for vapor qualities above 0.5.

As expected the HTC values obtained with the new correlations fit the experimental data much better than the other two correlations. However, for quality values close to 0 and to 1 these correlations can show some unrealistic variations (such as the sudden increase in HTC near 0 quality for correlation HTC3). This results from the fact that our experimental data does not cover these two extreme values, and extrapolating from strictly empirical correlations is not advised. Therefore, the proposed expressions should be used only if the input variables fall within the limits listed in Table A.1.

Table A.1
Input parameters considered in the search for the best HTC correlation.

X_i	Relation	Source	Range
1	$Re_{l,1} = G(1-x)\frac{d}{\mu_l}$	[29]	$[83, 33870]$
2	$\chi_{tt} = \left(\frac{1-x}{x}\right)^{0.875}\left(\frac{\rho_v}{\rho_l}\right)^{0.5}\left(\frac{\mu_l}{\mu_v}\right)^{0.125}$		$[1.8, 118.6]$
3	$Fr_l = \frac{G^2}{\rho_l^2 g\ d}$		$[0.01, 1.6]$
4	$UC_1 = 1 + 1.893\chi_{tt}^{-0.77}$		$[4.7\times10^{-3}, 3.0]$
5	$Re_{l,2} = \rho_l U_l \frac{d}{\mu_{eq}}$		$[4.5\times10^{3}, 2.5\times10^{5}]$
6	$Pr_{eq} = \mu_{eq}\frac{cp_{eq}}{k_{eq}}$		$[2.5\times10^{-4}, 11.1]$
7	$P_1 = \frac{i_{lv}}{U_l^2}$	[30]	$[7.7\times10^{5}, 1.4\times10^{8}]$
8	$P_2 = \frac{\sigma}{U_l\mu_{eq}}$		$[119.5, 7084]$
9	$Re_{l,3} = \rho_l U_v \frac{d}{\mu_{eq}}$		$[27.8, 70.2]$
10	$P_3 = \frac{dg}{U_l^2}$		$[1.8\times10^{5}, 1.2\times10^{7}]$
11	$P_4 = \frac{di_{lv}^{0.5}\rho_l}{\mu_{eq}}$		$[0.62, 9.0]$
12	$P_5 = \frac{U_l}{i_{lv}^{0.5}}$		$[3.3\times10^{7}, 3.3\times10^{8}]$
13	$P_6 = \frac{\sigma}{i_{lv}^{0.5}\mu_{eq}}$		$[8.6\times10^{-5}, 1.1\times10^{-3}]$
14	$P_7 = \frac{U_v}{i_{lv}^{0.5}}$		$[0.1, 1]$
15	$P_8 = di_{lv}^{0.5}\frac{\rho_v}{\mu_{eq}}$	[30]	$[3\times10^{-3}, 5\times10^{-2}]$
16	$P_9 = \frac{dg}{i_{lv}^{0.5}}$		$[4.9\times10^{5}, 10^{7}]$
17	$P_{10} = \frac{U_v}{U_l}$		$[6.4\times10^{-7}, 8\times10^{-7}]$
18	$C_1 = \frac{P}{P_{crit}}$	Present work	$[0.09, 0.2]$
19	$C_2 = \frac{\rho_v}{\rho_{crit}}$		$[0.03, 0.1]$
20	$C_3 = \frac{\rho_{eq}}{\rho_{crit}}$		$[0.18, 2.7]$
21	$C_4 = \frac{\rho_w}{\rho_{crit}}$		$[2.1, 2.75]$
22	$C_5 = \frac{T_l}{T_{crit}}$		$[0.06, 0.16]$
23	$\varepsilon = \frac{x}{\rho_v}\left\{[1+0.12(1-x)]\left(\frac{x}{\rho_v}+\frac{1-x}{\rho_l}\right)\frac{1.18(1-x)[g\sigma(\rho_l-\rho_v)]^{0.25}}{G\rho_l^{0.5}}\right\}^{-1}$	[26]	$[0.46, 1]$
24	$x_{IA} = \left\{\left[0.291\left(\frac{\rho_v}{\rho_l}\right)^{-0.571}\left(\frac{\mu_v}{\mu_l}\right)^{-0.143}\right]+1\right\}^{-1}$		$[0.32, 0.43]$
25	$Q_{crit} = \frac{0.131\rho_v^{0.5}i_{lv}[g\sigma(\rho_l-\rho_v)]^{0.25}}{\mathrm{W\ m^{-2}}}$		$[3.6\times10^{5}, 4.75\times10^{5}]$
26	$Bo = \frac{\phi}{Gi_{lv}}$	[29]	$[5\times10^{-5}, 1.3\times10^{-5}]$
27	$h_l = 0.023Re_l^{0.8}Pr_l^{0.4}\frac{k_l}{d}$		$[7, 943]$
28	$h_{nb} = 55P_r^{0.12}(-logP_r)^{-0.55}\times M^{-0.5}q^{0.67}$	[31]	$[1180, 4377]$

Table A.2
Values of weights and bias for the best ANN given by Eq. (8) for the correlation HTC4$_a$.

w_{ij}										w_{i0}	w_i	w_0
−0.1424	0.1922	0.4215	1.3803	−0.1452	0.1112	−0.5946	−0.7807	−0.4771	−0.1482	1.3209	−3.0945	−0.9915
1.7194	1.0551	2.6204	2.4736	−1.3256	−1.0862	0.0341	−0.4286	−0.7888	−1.2074	−1.9022	−1.6597	
0.7772	−3.2020	−0.7321	−0.0028	−1.5217	−1.8084	−0.5497	−1.4104	0.6144	1.0353	1.7100	2.1320	
0.3045	2.6936	−0.1265	−0.7760	−0.5178	−1.2630	−1.7385	−2.9066	0.2220	0.2152	−1.5628	4.8032	
−0.7424	0.3821	−3.6355	2.0113	1.0943	−0.2233	−1.1597	−1.3324	3.2705	−1.0704	−2.8557	−1.8039	
0.6111	0.0726	−0.6507	2.1626	−1.7451	−2.5551	2.0485	1.9788	0.2734	−0.1216	−2.4058	−2.5987	

6. Conclusions

This work demonstrates that more accurate and more robust correlations for two-flow heat transfer coefficients (HTCs) can be obtained successfully using advanced optimization techniques. A total of 690 data points covering a wide range of saturated two-phase flow regimes for refrigerants R-22, R-134a and R-404a were used to develop HTC correlations for evaporator tube flows. Four types of empirical correlations were developed from this unique data set. The different types of correlations were then optimized for 2 cases (except for the third correlations, which could only be applied to the first case). The first case assumes that the wall heat flux is known and the second case assumes that the wall heat flux is not known (a more common situation in heat transfer design).

We compared our proposed correlations against correlations available in the literature. Several error metrics indicate superior performance by the correlations proposed in this work. We also provided a more detailed comparison for R-22, by studying the correlations as a function of the flow patterns. We concluded that the correlations HTC1$_a$, HTC3 and HTC4$_b$ offer substantially better performance in fitting the R-22 data for all the mass flow rate cases under study than other correlations from the literature. Our results emphasize that, despite the best performance of the proposed correlations, care should be exercised when extrapolating these or any other empirical correlations for vapor quality values that lie beyond the limits under study in the original test sets.

Appendix A

A.1. Error metrics

The error metrics used to assess the performance of the proposed correlations are:

1. Mean Absolute Error,

$$\mathrm{MAE} = \frac{1}{N}\sum_{i=1}^{N}|y_i - \hat{y}_i|. \tag{A.1}$$

2. Mean Bias Error,

$$\mathrm{MBE} = \frac{1}{N}\sum_{i=1}^{N} y_i - \hat{y}_i. \tag{A.2}$$

3. Root Mean Square Error,

$$\mathrm{RMSE} = \sqrt{\frac{1}{N}\sum_{i=1}^{N}(y_i - \hat{y}_i)^2}. \tag{A.3}$$

4. Coefficient of determination,

$$\mathrm{R}^2 = 1 - \frac{\sum_{i=1}^{N}(y_i - \hat{y}_i)^2}{\sum_{i=1}^{N}(y_i - \bar{y})^2}, \tag{A.4}$$

where y is the measured HTC and $\hat{y}$ is the HTC computed with the new correlations, $\bar{y} = \frac{1}{N}\sum_{i=1}^{N} y_i$ and N is number of data points.

A.2. Input parameters

The input parameters candidate to be used in the correlations are listed in Table A.1. For each parameter, it is listed its definition, the source (if necessary) and the range that parameter takes for the 690 experimental data points used in this work.

Table A.3
Values of weights and bias for the best ANN given by Eq. (8) for the correlation HTC4$_b$.

w_{ij}													w_{i0}	w_i	w_0
2.4286	−0.1362	−0.4501	−0.7943	0.9822	−2.2125	1.0344	0.0167	−0.0959	−2.6176	1.1849	−0.5677	−0.3342	−1.0908	0.722	−0.3519	2.6319	−2.951	3.1624	−1.3939
−0.325	0.6662	0.5531	0.1966	0.2715	−0.9369	0.0508	0.1013	−0.539	0.9857	0.0661	−0.5679	−0.5416	0.2026	−0.2534	0.489	0.8596	1.5348	1.7309	
−0.4885	−0.8334	0.3488	−0.2567	0.5197	−0.134	0.0105	−0.9314	0.5974	0.4903	−0.1002	0.6868	−0.4358	1.5999	0.1749	−0.781	−0.0366	0.0655	−1.457	
1.1749	−0.6433	−0.2784	−0.4257	−0.2964	−0.3619	0.5246	1.0685	−0.083	−0.285	−1.1665	0.3223	1.0244	−0.9773	0.6086	0.414	0.3618	−0.8431	−2.3101	
1.7076	1.5716	0.4246	−0.6622	0.7783	−2.1139	0.0629	−0.4746	−0.1615	−1.7409	0.4508	−0.7764	−0.6658	−1.3834	−0.0546	−0.5307	1.943	−2.2114	−3.14	
0.9781	1.9919	1.926	−0.3857	−0.0651	0.5597	−0.8157	1.0062	−0.0219	−0.0818	−0.5073	−2.9523	0.1263	0.7142	−0.5371	−0.5822	−0.4923	1.0897	−1.432	
1.2704	0.6883	0.9909	−0.3227	−0.3761	−0.3509	−0.2362	2.3484	−0.0347	0.1135	−1.3441	−0.1947	1.1623	0.361	0.215	0.2103	0.0601	0.9473	1.6518	

A.3. ANN weights and bias

Tables A.2 and A.3 list the weights and bias for the ANN-based correlations. These values, Eq. (8) and the information in Table 3 determine the correlations HTC4$_a$ and HTC4$_b$, respectively.

References

[1] L. Gosselin, M. Tye-Gingras, F. Mathieu-Potvin, Review of utilization of genetic algorithms in heat transfer problems, Int. J. Heat Mass Transfer 52 (2009) 2169–2188.

[2] M. Mohanraja, S. Jayaraj, C. Muraleedharanb, Applications of artificial neural networks for refrigeration, air-conditioning and heat pump systems – a review, Renewable Sustainable Energy Rev. 16 (2012) 1340–1358.

[3] K. Jambunathan, S.L. Hartle, S. Ashforth-Frost, V.N. Fontama, Evaluating convective heat transfer coefficients using neural network, Int. J. Heat Mass Transfer 39 (1996) 2329–2332.

[4] G. Scalabrin, L. Piazza, Analysis of forced convection heat transfer to supercritical carbon dioxide inside tubes using neural networks, Int. J. Heat Mass Transfer 46 (2003) 1139–1154.

[5] W. Wang, L. Zhao, C. Zhang, Generalized neural network correlation for flow boiling heat transfer of R22 and its alternative refrigerants inside horizontal smooth tubes, Int. J. Heat Mass Transfer 49 (2006) 2458–2465.

[6] C.U.S. Lima. Convective boiling of refrigerants flowing in copper horizontal tubes, Ph.D. Thesis, University of São Paulo, São Carlos School of Engineering, São Paulo, Brazil, 2000.

[7] M.A.S. Picanço, E.P.F. Bandarra, J.C. Passos. Heat transfer coefficient correlation for convective boiling inside plain and microfin tubes using genetic algorithms, in: Proceedings of the 11th Brazilian Congress of Thermal Sciences and Engineering? ENCIT, Braz. Soc. of Mechanical Sciences and Engineering? ABCM, Brazil, 2006.

[8] F.P. Incropera, D.P. deWitt, T. Bergman, A. Lavine, Fundamentals of Heat and Mass Transfer, John Wiley Sons, Jefferson City, 2007.

[9] J.N. Addoms, C.E. Dengler, Heat transfer mechanism for vaporization of water in a vertical tube, Chem. Eng. Prog. Symp. 52 (1956) 95–103.

[10] S.A. Guerrieri, R.D. Talty, A study of heat transfer to organic liquids in a single tube, natural circulation, vertical tube boilers, Chem. Eng. Prog. Sym. Ser. 56 (1956) 69–77.

[11] J.B. Chaddock, J.A. Noerager, Evaporation of R-12 in a horizontal tube with constant heat flux, ASHRAE Trans. 72 (1966) 99–103.

[12] J.B. Chaddock, G. Buzzard, Film coefficients for in-tube evaporation of ammonia and R502 with and whitout small percentages of mineral oil, ASHRAE Trans. 92 (1986) 22–40.

[13] J. Panek. Evaporation heat transfer and pressure drop in ozone-safe refrigerants and refrigerant-oil mixtures, Ph.D. thesis, University of Illinois at Urbana-Champaign, 1992.

[14] F.E.P. Bandarra. Study of convective boiling heat transfer of halocarbon refrigerants in horizontal tubes, Master's Thesis, Escola de Engenharia de São Carlos, Universidade de São Paulo, 1997.

[15] F.W. Dittus, L.M.K. Boelter, Heat transfer in automobile radiators of the tubular type, Univ. California Publ. Eng. 2 (1930) 443–461.

[16] J.M.S. Jabardo, F.E.P. Bandarra, C.U.S. Lima, A new correlation for convective boiling of pure halocarbon refrigerants? Owing in horizontal tubes, Braz. J. Mech. Sci. 21 (1999) 245–258.

[17] J.C. Chen. A correlation for boiling heat transfer to saturated fluids in convective flow, in: Sixth National Heat Transfer Conference, 1963, pp. 11–14.

[18] K.E. Gungor, R.H.S. Winterton, A general correlation for flow boiling in tubes and annuli, Int. J. Heat Mass Transfer 29 (1986) 351–358.

[19] K.E. Gungor, R.H.S. Winterton, Simplified general correlation for saturated flow boiling and comparison of correlations to data, Chem. Eng. Res. Des. 65 (1987) 148–156.

[20] J.P. Wattelet, Heat transfer flow regimes of refrigerants in a horizontal-tube evaporator, Ph.D. Thesis, University of Illinois at Urbana-Champaign, 1994.

[21] D. Jung, R. Radermacher, Prediction of evaporation HTC and pressure drop of refrigerant mixtures, Int. J. Refrig. 16 (1993) 330–338.

[22] Z. Liu, R.H.S. Winterton, A general correlation for saturated and subcooled flow boiling in tubes and annuli, based on a nucleate pool boiling equation, Int. J. Heat Mass Transfer 34 (1991) 1759–2766.

[23] B. Pierre, Coefficient of heat transfer for boiling freon-12 in horizontal tubes, Heat. Air Treat. Eng. 19 (1956) 302–310.

[24] S.G. Kandlikar, A general correlation for saturated two-phase flow boiling heat transfer inside horizontal and vertical tubes, J. Heat Transfer 112 (1990) 219–228.

[25] M.M. Shah, Chart correlation for saturated boiling heat transfer: equations and further study, ASHRAE Trans. 88 (1982) 302–310.

[26] Y. Taitel, A.E. Dukler, A model for predicting flow regime transitions in horizontal and near horizontal gas? Liquid flow, AIChE J. 22 (1976) 47–55.

[27] O. Baker, Design of pipe lines for simultaneous flow of oil and gas, Oil Gas J. 53 (1954) 185–190.

[28] D. Steiner, VDI-Wärmeatlas (VDI Heat Atlas), Verein Deutscher Ingenieure, VDI-Gesellschaft Verfahrenstechnik und Chemieingenieurwesen (GCV), Düsseldorf, 1993.

[29] N. Kattan, J.R. Thome, D. Favrat, Flow boiling in horizontal tubes. Part 1: Development of a diabatic two phase flow pattern map, J. Heat Transfer 120 (1998) 140–147.

[30] N. Kattan, J.R. Thome, D. Favrat, Flow boiling in horizontal tubes. Part 3: Development of a new heat transfer model based on flow pattern, Braz. J. Mech. Sci. 120 (1998) 156–165.

[31] L. Wojtan, T. Ursenbacher, J.R. Thome, Investigation of flow boiling in horizontal tubes. Part I: A new diabatic two-phase flow pattern map, Int. J. Heat Mass Transfer 48 (2005) 2955–2969.

[32] L. Wojtan, T. Ursenbacher, J.R. Thome, Investigation of flow boiling in horizontal tubes: Part II: Development of a new heat transfer model for stratified-wavy, dryout and mist flow regimes, Int. J. Heat Mass Transfer 48 (2005) 2970–2985.

[33] T. Ursenbacher, L. Wojtan, J.R. Thome, Interfacial measurements in stratified types of flow. Part I: New optical measurement technique and dry angle measurements, Int. J. Multiphase Flow 30 (2004) 107–124.

[34] M.K. Cooper, Saturated nucleate pool boiling: a simple correlation, First UK Natl. Heat Transfer Conf. 2 (1984) 785–793.

[35] R. Fletcher, Practical Methods of Optimization, John Wiley and Sons, New York, 1987.

[36] C.M. Bishop, Neural networks and their applications, Rev. Sci. Instrum. 65 (6) (1994) 1803–1832.

[37] J.H. Holland, Adaptation in Natural and Artificial Systems, MIT Press, Cambridge, MA, 1992.